



The +2 oxidation state of Cr incorporated into the crystal lattice of UO_2

Mengli Sun ^{1,2,3}, Joshua Stackhouse^{1,2,4} & Piotr M. Kowalski ^{1,2}✉

Doping by Cr is used to improve the performance of uranium dioxide (UO_2)-based nuclear fuel. However, the mechanism of structural incorporation of Cr remains unclear. Here, in order to understand this process on the atomic scale and the redox state of Cr in UO_2 -based nuclear fuel, we performed intensive ab initio atomistic simulations of the Cr doped UO_2 matrix. We unexpectedly found that Cr in UO_2 exists as Cr^{2+} species and not as the widely claimed Cr^{3+} . We re-evaluated previously published x-ray absorption near edge structure spectroscopy data and confirmed the computed redox state of Cr. Thermodynamic consideration shows that the favorable structural arrangement of Cr in UO_2 is given by a pair of associated Cr^{2+} and oxygen vacancy. The realism of this doping mechanism is further demonstrated by a match to the measured maximum Cr solubility and small lattice contraction.

¹Institute of Energy and Climate Research (IEK-13 & IEK-6), Forschungszentrum Jülich, Wilhelm-Johnen-Straße, 52425 Jülich, Germany. ²JARA High-Performance Computing, Schinkelstraße 2, 52062 Aachen, Germany. ³School of Nuclear Science and Technology, Lanzhou University, Tianshui South Road 222, 730000 Lanzhou, China. ⁴Colorado School of Mines, 1500 Illinois Street, Golden, CO 80401, USA. ✉email: p.kowalski@fz-juelich.de

Nuclear reactors use mainly UO_2 -based fuel elements. Additions of other trace elements, such as chromium, are considered to improve the microstructural and mechanical properties of fuel matrices^{1,2}. Among other desired effects, chromium is known to significantly increase the grain sizes, which due to the elongation of bulk diffusion path limits the release of fission gas products such as xenon or krypton², and increases the fission products retention capability by the fuel elements³. However, how Cr incorporates into the UO_2 matrix on the atomic level is not conclusively understood. The impact of Cr doping on the performance of UO_2 matrix depends also on the oxidation state of Cr in the nuclear fuel, which is claimed to be Cr^{3+} ^{4,5}. Other oxidation states, however, are not excluded^{6,7}. In particular, by analyzing X-ray absorption spectrum of Cr-doped UO_2 Mieszczynski et al.⁷ suggest existence of Cr^{2+} , but express a need for the electronic structure calculations to confirm such a possibility.

The most common oxidation states of chromium are Cr^{3+} and Cr^{6+} . However, the Cr^0 , Cr^{1+} , Cr^{2+} , Cr^{4+} , or Cr^{5+} could be also realized⁸. The previous experimental studies of Cr-doped UO_2 show evidence of bulk Cr incorporation as Cr^{3+} ⁴. At the same time, only small amounts of Cr could be incorporated into UO_2 , with maximum solubility at high temperature ($T \sim 2300$ K) of up to 0.1 wt% UO_2 ^{3-5,9}. The formed diluted solid solution shows a linear decrease in the matrix lattice parameter with content of Cr^{1,9}, which however, is significantly smaller than the predictions by most theoretical models¹.

Besides the experimental effort, the atomistic modeling studies have been used to understand the incorporation of Cr into the UO_2 matrix at atomic level. Most of these studies used force-fields approach, in which interatomic interactions are represented by analytical functions and charge/oxidation states of the involved species are fixed¹⁰, for chromium atom to Cr^{3+} ^{1,11,12}. Middleburgh et al.¹² and more recently Guo et al.¹¹ found that Cr incorporates as a pair of Cr atoms with the formation of an oxygen vacancy (on the oxygen site that bridges the two Cr atoms) as a charge balance mechanism. The density functional theory (DFT)-based first principles studies of Middleburgh et al.¹² consider formation of Cr^{3+} as dominant Cr species in the same structural arrangement as resulted from the force-field simulations, and discuss a less energetically favorable scenario of Cr^{4+} . The more recent ab initio studies of Cooper et al.⁶ show the possibility of Cr in “+1” oxidation state. Interestingly, the “+2” state has never been considered as dominant at ambient or high-temperature synthesis conditions ($T > 1500$ K). The oxidation state chemistry of uranium oxides is very interesting with different oxides realizing uranium in different oxidation states (U^{4+} , U^{5+} , or U^{6+}), for instance U_3O_8 and U_4O_7 as mixtures of (U^{6+} , U^{5+}) and (U^{5+} , U^{4+}) pairs, respectively¹³⁻¹⁵. Potential change in the cations redox states would have a significant impact on the evolution of nuclear fuel, including, for instance, its dissolution rates^{16,17}. The real oxidation states are not always well constrained, but could be conclusively deduced by a combination of X-ray absorption near edge structure (XANES) measurements and first-principle atomistic modeling¹⁵. It is also not conclusively clear, how different impurities or defects affect oxidation states of the UO_2 matrix atoms.

Here, we present the atomistic modeling studies combined with an extensive analysis of the relevant experimental data (XANES, the maximum solubility and the lattice parameter), aimed at understanding the atomic structure and redox chemistry of Cr-doped UO_2 material. We have been especially interested in the resulting oxidation state of Cr and U cations, derivation of the conclusive structural model of Cr incorporation and testing the ability of such a model structure to match the measured solubility limit of Cr in UO_2 and the lattice parameter of Cr-doped UO_2 matrix.

Results

The computed Cr-doped UO_2 . In order to perform the DFT+ U calculations, we first derived the Hubbard U parameter for the d and f elements in the considered compounds (Cr and U oxides, see Fig. 1 for the computed structure of UO_2). The computed value of Hubbard U parameter for Cr in Cr_2O_3 (i.e., Cr^{3+}) is 4.0 eV, which is consistent with the one used in previous studies of Cr-bearing systems (~ 3.5 eV, e.g., refs. 6,18–21). For Cr^{2+} we used the value of 6.5 eV, which we derived for CrO. The same value we were getting for Cr^{2+} in UO_2 and we observed that the derived Hubbard U parameter depends strongly on the Cr oxidation state, but is weakly dependent on the local environment of Cr. Therefore, we decided to use the oxidation state-dependent values derived for Cr-oxides in all the calculations of Cr-doped UO_2 . For UO_2 we used 1.7 eV derived for UO_2 by Beridze and Kowalski²², which is also representative for U^{4+} species^{15,22,23}. The detailed information and discussion on the lattice parameter, the band gap and the X-ray related spectral signatures obtained for UO_2 , as well as other uranium oxides with the applied computational methodology is provided in the previous studies^{15,22}.

Initially, we computed the two most plausible cases of Cr-doped UO_2 , namely: (1) the cation exchange with the formation of U^{5+} species and (2) the two neighboring site cation exchange with the formation of O-vacancy on the bridging oxygen site attached to the Cr atoms as proposed by Guo et al.¹¹. Both configurations are visualized in Fig. 2 and are marked as 1Cr and 2Cr + 1Ov, respectively. Following the interpretation of XANES measurements by Riglet-Martial et al.⁴, in both cases we initially assumed formation of Cr^{3+} species. In the case (1) we assumed the charge balance through formation of one U^{5+} per one Cr atom. In addition, for the case (1) we tried to compute systems with Cr^{2+} and Cr^{4+} species, by enforcing the initial occupation of d -orbitals of Cr (4, 3, and 2 d electrons for Cr^{2+} , Cr^{3+} , and Cr^{4+} , respectively). Surprisingly, in all the calculations, the resulting electronic configuration was always that of Cr^{2+} (i.e., four electrons), with charge balanced by the formation of U^{5+} species.

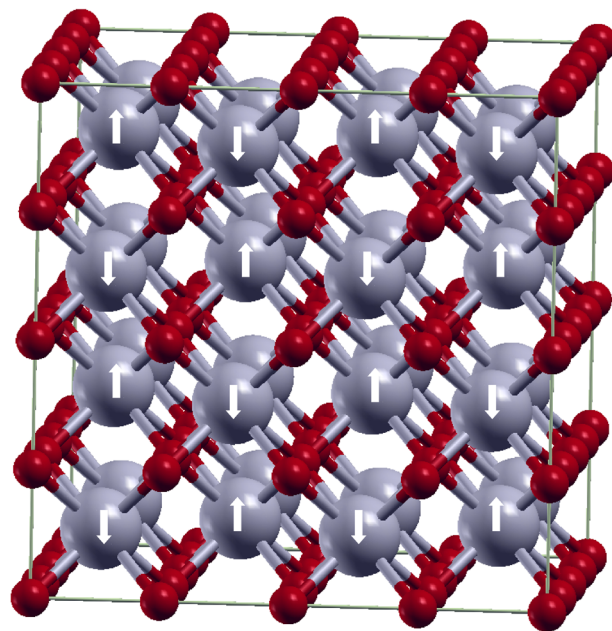


Fig. 1 The structure of computed UO_2 supercell. Arrows indicate the computed transverse 1k anti-ferromagnetic spin arrangement, which was found by Pegg et al.⁵² as the preferred magnetic structure in UO_2 and adopted in our studies.

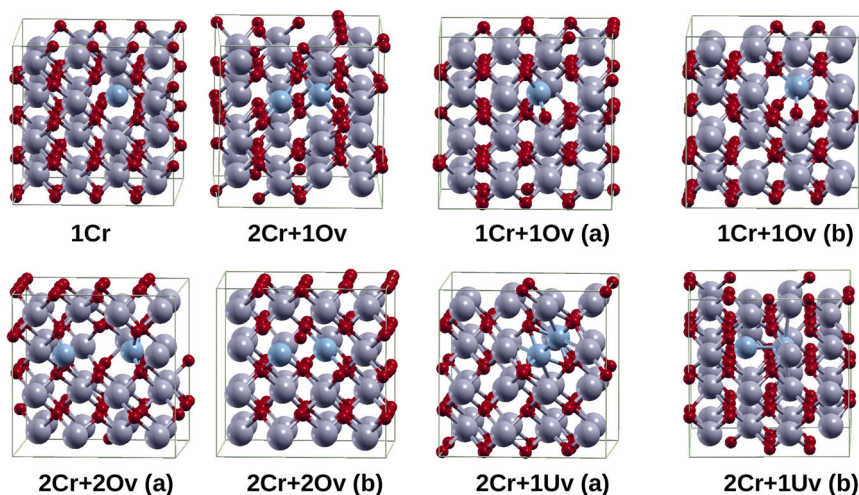


Fig. 2 The computed supercells representing different considered Cr incorporation configurations. In cases of 1Cr+10v (a) and 2Cr+20v (a) Cr is shifted towards empty cation interstitial site and the two structures resulted from classical molecular simulation runs.

Table 1 The ionic radius (r), and volume (V) of Cr and U cations in different oxidation state.

Cation	r (6)	V (6)	r (8)	V (8)
Cr ²⁺	0.80	2.14	0.88	2.85
Cr ³⁺	0.62	1.00	0.70	1.44
U ⁴⁺	0.89	2.95	1.00	4.19
U ⁵⁺	0.76	1.84	0.89	2.95

The values are given in Å and Å³, respectively. Cases of 6- and 8-fold coordinated cations are reported with coordination number given in parentheses.

For instance, in case (2) with the formation of two Cr²⁺ species we got a pair of U⁵⁺.

Such an unexpected theoretical result requires sounding justification and support from the experimental data. The simplest thing to do, when considering oxidation state of a species substituting another host matrix element, i.e., chromium substituting uranium atom in our case, is to check the sizes of involved cations. This is because it is easier to exchange cations of similar sizes due to minimization of the associated strain resulting from sizes mismatch. In Table 1, we list the ionic radii and volumes of the considered species²⁴. Cr³⁺ is much smaller than U⁴⁺ (by 66% in volume) and even U⁵⁺ (by 51% in volume). The size of Cr²⁺ is much similar to that of U⁴⁺ (smaller by only 32% in volume) and nearly the same as that of U⁵⁺. As excess strain effects arise as quadratic function of volume mismatch (e.g., Kowalski and Li²⁵), considering the sizes of cations, the scenario with Cr²⁺ is more probable. However, even with appealing theoretical arguments in hand, one can not easily neglect the results of XANES studies of Riglet-Martial et al.⁴ that seem rather conclusively indicate formation of Cr³⁺ in Cr-doped UO₂. Therefore, we decided to perform re-analysis of these data using the reference XANES for Cr²⁺, the case that is missing in the analysis of Riglet-Martial et al.⁴

The re-evaluation of the experimental XANES. The oxidation state of an atom in a solid matrix is usually measured with the help of XANES technique²⁶. For that purpose, the measured data are compared to a set of reference data of a species in different oxidation state. In the previous studies of Riglet-Martial et al.⁴, the references for Cr⁰ (Cr metal), Cr³⁺ (Cr₂O₃, FeCrO₄), and

Cr⁶⁺ (CaCrO₄) were used for analysis of XANES of Cr-doped UO₂. The authors concluded that their XANES of Cr-doped UO₂ resembles best the reference for Cr³⁺, which they use as a definitive evidence for the existence of Cr³⁺ in UO₂. The conclusion is mainly supported by the best match of the positions of two pre-edges, which follows from the in-depth characterization of XANES spectra of various Cr-bearing compounds by Farges²⁷. However, the match to the reference XANES is not ideal, which suggest possible other interpretation. In similar studies, Mieszczyński et al.⁷, although assumed Cr³⁺, also discuss possibility of existence of Cr²⁺ state, which could be indicated by a shoulder feature at 5996 Å, marked by the arrow in Fig. 3. In order to confirm or reject the possible Cr²⁺ state scenario they expressed a need for ab initio calculations. As such simulations performed here show definitely the Cr²⁺ state, we made an extensive literature search for a relevant reference for Cr²⁺ state. We found such data on Cr²⁺ in synthetic enstatite (Mg_{0.9}Cr_{0.1}SO₃)²⁸. With these, in Fig. 3 we plot the XANES of Cr-doped UO₂ of Riglet-Martial et al.⁴, which are consistent with the data of Mieszczyński et al.⁷, together with the reference data for Cr³⁺ (Cr₂O₃) and for the aforementioned Cr²⁺. The comparison of the entire spectra shows that the XANES measured by Riglet-Martial et al.⁴ resembles as closely the Cr³⁺ as Cr²⁺ references. This refers to the spectral shape and the distribution of peaks and dips, that are, anyway, not perfectly reproduced by the references. This “imperfectness” is rather expected and, as explained by Farges²⁷, comes from the different local environments of Cr in all the considered phases. Following analysis of Farges²⁷, applied also by Riglet-Martial et al.⁴, it is the positions of the two pre-edges, or weighted centroids (of the peaks located at ~5991 eV and ~5994 eV in the case of Cr₂O₃, Fig. 3) that discriminate between the different oxidation states of Cr. There is a significant and progressive shift in the second pre-edge peak (the higher energy peak) and centroid positions as a function of Cr oxidation state (~1 eV per increase in the oxidation state). For different Cr species, the centroid should be located as follows: ~5993 eV (Cr²⁺), ~5994 eV (Cr³⁺), ~5995 eV (Cr⁴⁺), ~5995.7 eV (Cr⁵⁺) and ~5996.7 eV (Cr⁶⁺) (see Fig. 4 of Farges²⁷). We thus have checked the position of that centroid in XANES of Cr-doped UO₂ and compared it to the references for Cr²⁺ and Cr³⁺. The positions of the first, lower energy pre-edge peak are very similar for both oxidation states of Cr²⁺ (See Fig. 3 and Supplementary Fig. 1). We note that the comparison to the Cr²⁺ reference was not performed by Riglet-Martial et al.⁴

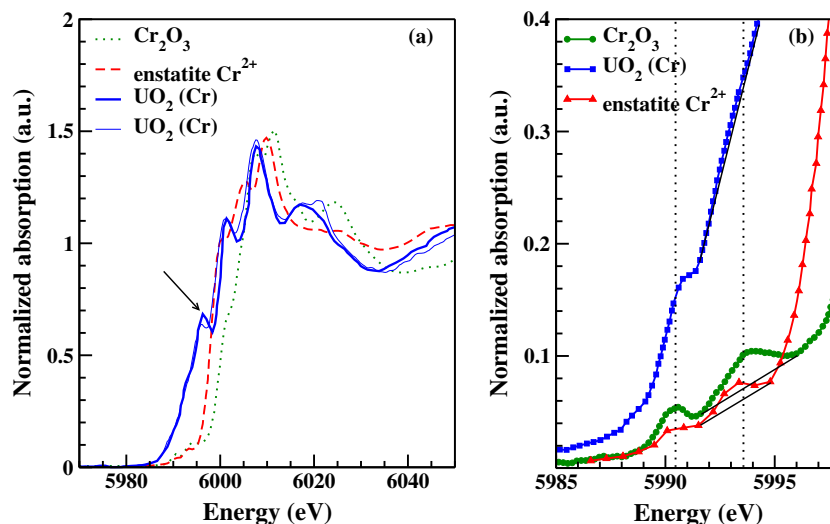


Fig. 3 The XANES spectra of the Cr-doped UO_2 . **a** The spectra of the Cr-doped UO_2 (thick solid blue line)⁴ and (thin solid blue line)⁷, and reference phases for Cr^{2+} ²⁸ and Cr^{3+} ⁴; **b** the pre-edge region of the spectra. The black solid and dotted lines in **b** represent the linear baselines used for extraction of the second pre-edge feature peak and positions of the two pre-edges peaks as indicated by Riglet-Martial et al.⁴ (their Fig. 2b). We note very good agreement between the two independent measurements of the XANES spectra of the Cr-doped UO_2 ^{4,7}. The arrow indicates the pre-edge 5996 Å feature speculated by Mieszczyński et al.⁷ to be a signature of the Cr^{2+} .

As shown in Fig. 3, the second pre-edge peak that discriminates the different Cr species is located at ~ 5993 eV for Cr^{2+} and ~ 5994 eV for Cr^{3+} species, and the offset of ~ 0.7 eV is clearly visible. On the other hand, that peak is barely visible, but clearly detectable (Fig. 3) in the spectra of Cr-doped UO_2 of Riglet-Martial et al.⁴. In order to check the right position of that pre-edge peak, we isolated the relevant peak from the spectra by subtracting out a linear baseline that spans the base of the feature. The obtained profiles of the peaks for the Cr^{2+} and Cr^{3+} references and the Cr-doped UO_2 XANES spectra are compared in Fig. 4. The three peaks extracted from XANES are symmetric, which is demonstrated with good fits by the Gaussian (see Supplementary Table 1 for the fitted parameters). This also validates the applied data processing procedure. It is clearly visible that the position and height of the peaks of Cr^{2+} and the Cr-doped UO_2 are similar and the position of the peak in the case of Cr^{3+} is significantly shifted rightwards by ~ 0.7 eV. The so derived second pre-edge positions obtained by fitting with Gaussian function are given in Table 2. Here, we also report the positions of centroid (i.e., a weighted average of the all pre-edge peaks) obtained using the multi-peaks fitting procedure proposed by Farges²⁷ and Wilke et al.²⁹ (see Supplementary Note 1 and Supplementary Tables 2 and 3 for details).

The obtained positions of the pre-edge centroid were then compared with the results obtained by Farges²⁷ for the set of Cr-materials containing Cr in different oxidation states ranging from “+2” to “+6”. The results are given in Fig. 5, which resembles Fig. 4 of Farges²⁷. The positions of centroids we got for the Cr^{2+} and Cr^{3+} references (Table 2) fell within the given ranges of Farges²⁷, indicating agreement with that data. The centroid position in the case of Cr-doped UO_2 falls in the range corresponding to Cr^{2+} . The careful analysis of the pre-edge XANES spectrum of Cr-doped UO_2 shows thus rather clearly the “2+” oxidation state of chromium in Cr-doped UO_2 .

Both, the above-discussed atomistic simulations and the experimental XANES data thus clearly indicate incorporation of chromium into UO_2 matrix as Cr^{2+} species. This must be associated with the formation of U^{5+} species or O vacancies. This may affect the overall performance of such material, including its dissolution rate, which strongly depends on the U oxidation

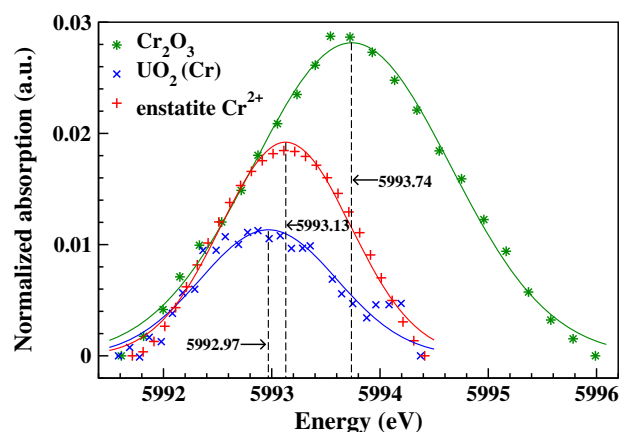


Fig. 4 The extracted XANES pre-edges peaks for Cr-doped UO_2 , and reference Cr^{2+} and Cr^{3+} structures. The energy resolution of the measured spectra of Cr-doped UO_2 is estimated at 0.3 eV⁴. This permits accurate fits of the pre-edge peak positions and conclusive identification of the clear offsets from the reference spectra.

states^{30,31}. In order to predict the most probable structural arrangement of Cr in UO_2 matrix we computed a set of simple, different Cr incorporation arrangements involving single, as well as pair of dopants with charge balancing through formation of oxygen vacancies (Ov) or U^{5+} species. The eight computed configurations are visualized in Fig. 2 and some of them (e.g., $1\text{Cr}+1\text{Ov}$ (a) and $2\text{Cr}+2\text{Ov}$ (a)) were obtained with the aid of classical molecular dynamics simulations. All the constructed supercells were then carefully analyzed regarding the enthalpy and the free energy of relevant cation exchange reaction and the change in the matrix lattice parameter. The obtained results were analyzed against the available experimental data on the maximum solubility (requiring the reaction enthalpy and the free energy as parameters)^{1,4,9,32,33} and change in the lattice parameter of Cr-doped UO_2 ^{1,9}.

The Cr solubility limit in UO_2 . Riglet-Martial et al.⁴ derived a simple thermodynamic model of maximum Cr solubility in UO_2 ,

Table 2 The position of the second pre-edge peak feature obtained by fits by Gaussian function ($A \exp(B(x - C)^2)$) as illustrated in Fig. 4 and the position of the centroid.

Materials	Second pre-edge peak position	Centroid position
Cr-doped UO_2	5992.97 ± 0.10	5992.66 ± 0.02
Cr^{2+} enstatite	5993.13 ± 0.03	5992.16 ± 0.04
$\text{Cr}^{3+}\text{Cr}_2\text{O}_3$	5993.74 ± 0.05	5993.50 ± 0.02

The values are given in eV. The errors of the fitted values are comparable to those obtained by Farges²⁷ (0.05 eV).

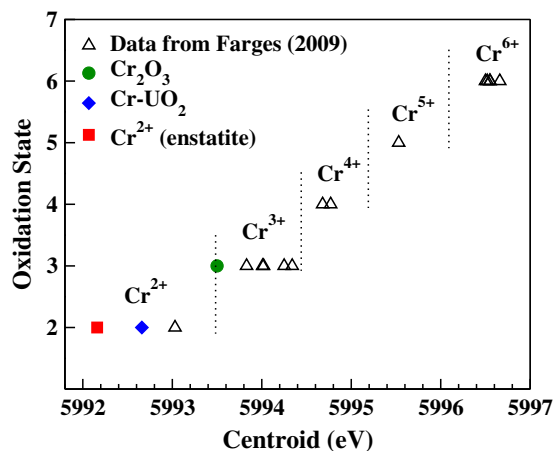
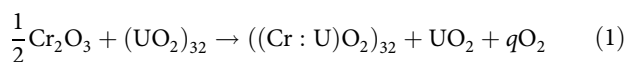


Fig. 5 The pre-edge centroid positions for the Cr in different oxidation states varying from “+2” to “+6”. The data represented by black triangles come from ref. ²⁷. The blue diamond is the result for Cr-doped UO_2 and the green circle and red square are the result for Cr^{3+} and Cr^{2+} references.

which when fitted to the measured temperature dependent maximum Cr solubility in UO_2 ^{4,9,32,33} resulted in the estimation of Cr solution enthalpy and entropy (Table 5 of Riglet-Martial et al.⁴). The result depends on the Cr-oxide reference phase and for Cr_2O_3 they obtained the reaction enthalpy of 92.4 kJ mol^{-1} , assuming Cr^{3+} incorporation into UO_2 . In Table 3 we provide the enthalpy of single Cr atom solution computed ab initio, assuming the following cation exchange reactions (having the size of computed supercell as 32 UO_2 units), realizing eight considered structural arrangements of Cr in UO_2 (Fig. 2):



In addition, in Table 3 we report an estimate for the Cr solution free energy (ΔG), which we derived by adding/subtracting the high-temperature entropy of molecular oxygen gas ($S(\text{O}_2) = 270 \text{ J mol}^{-1} \text{ K}^{-1}$, Chase³⁴) and the oxygen partial pressure contribution to the free energy. Depending on the involvement of molecular oxygen as product or reactant, the free energy is estimated from:

$$G = H - TS + q(RT \ln 10) \log_{10} P_{\text{O}_2}, \quad (2)$$

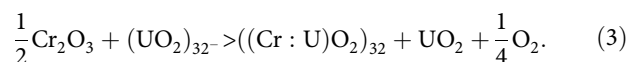
where $\Delta S \approx qS(\text{O}_2)$ and ΔH is the enthalpy of single cation exchange reaction (Eq. (1)). The temperature dependent oxygen partial pressure was estimated using the model of Toker et al.³⁵ and the values used in the calculations are reported in caption of Table 3.

Table 3 The computed solution enthalpy, ΔH , and free energy, ΔG , of Cr in UO_2 .

Configuration	ΔH	$\Delta G (T = 1800 \text{ K})$	$\Delta G (T = 2200 \text{ K})$
1Cr	82	333	344
2Cr+1Ov	168	168	168
1Cr + 1Ov (a)	327	95	84
1Cr+1Ov (b)	328	96	85
2Cr+2Ov (a)	387	155	144
2Cr+2Ov (b)	384	152	141
2Cr+1Uv (a)	418	650	661
2Cr+1Uv (b)	620	852	863

The values are given in kJ mol^{-1} and computed per single Cr atom. The bold face font indicates the thermodynamically favorable structure. The oxygen partial pressures used in the estimation of the free energies are $\log_{10} P_{\text{O}_2} = -12.85$ ($T = 1800 \text{ K}$) and $\log_{10} P_{\text{O}_2} = -9.01$ ($T = 2200 \text{ K}$)³⁵.

The derived reaction enthalpies suggest that the 2Cr+1Ov incorporation mechanism is the most preferable, which is in line with the prediction of Guo et al.¹¹. However, the reaction free energy—a more relevant parameter—points towards 1Cr+1Ov and 2Cr+2Ov scenarios, with the 1Cr+1Ov being the most preferable. We thus assume that Cr incorporates as an associated pair of Cr and Ov, and focus on checking the performance of the two structures (1Cr+1Ov (a) and 1Cr+1Ov (b), Fig. 2) in matching the measured solubility data. For that case we consider the following cation exchange reaction:



The activity, a , of Cr in UO_2 is related to the oxygen gas partial pressure and the cation exchange reaction enthalpy and entropy as (Riglet-Martial et al.⁴, Eq. (6)):

$$\log_{10}(a(\text{Cr} : \text{UO}_2)) = q \log_{10} P_{\text{O}_2} + \frac{1}{R \ln 10} (S - H/T). \quad (4)$$

The 1Cr+1Ov structure represents a pair of Cr atom and associated Ov. In that case, for cubic fluorite structure, the activity of Cr in UO_2 is $a(\text{Cr} : \text{UO}_2) = (y/8)$, where y is the concentration of Cr in UO_2 . This is because an associated Ov has eight possibilities to arrange around the Cr atom (the case of a cube with Cr atom in the center and eight oxygen atoms in the corners), This gives the following equation for the maximum solubility of Cr in the case of 1Cr+1Ov structural arrangements:

$$\log_{10}(y) = -\frac{1}{4} \log_{10} P_{\text{O}_2} + \frac{1}{R \ln 10} (S - H/T) + \log_{10} 8. \quad (5)$$

The 2Cr+2Ov structure represents a pair of associated Cr atoms with removed two oxygen atoms that bridge the Cr atoms. In that case, for cubic fluorite structure, the activity of Cr in UO_2 is $a(\text{Cr} : \text{UO}_2) = (y/12)^{1/2}$. This is because for a pair of associated Cr atoms, second Cr atom has 12 possibilities to be arranged around the first Cr atom (the two Cr atoms are connected by a cube edge and there are 12 such arrangements (edges)), and the activity of a single atom is just the square root of the activity of a pair. This gives the following equation for the maximum solubility of Cr in the case of 2Cr+2Ov structural arrangement:

$$\log_{10}(y) = -\frac{1}{2} \log_{10} P_{\text{O}_2} + \frac{2}{R \ln 10} (S - H/T) + \log_{10} 12. \quad (6)$$

The resulted Cr solubility, y , estimated for the conditions of various measurements reported in the literature, by applying the two discussed structural arrangement models and the computed cation exchange reaction enthalpies (Table 3) along with the experimental oxygen partial pressures, are given in Table 4. We note that such an estimate in the case of the preferred 1Cr+1Ov model, with the computed here ΔH , only slightly overestimates the

Table 4 The computed and measured maximum solubility (y) of Cr in UO_2 reported for the experimental conditions.

T (°C)	μ_{O_2}	$\log_{10} P_{\text{O}_2}$	$\log_{10} y$ (exp)	M1:	$\log_{10} y$	ΔH (exp)	$\log_{10} y_e$	M2:	$\log_{10} y$	ΔH (exp)	$\log_{10} y_e$
1655	-386.5	-10.47	-2.36 ⁴		-1.81	347	-2.35		-7.44	290	-2.35
1655	-386.5	-10.47	-2.31 ⁴		-1.81	346	-2.33		-7.44	289	-2.29
1600	-403.2	-11.24	-2.47 ⁹		-1.88	348	-2.46		-7.66	291	-2.48
1660	-399.7	-10.80	-2.35 ⁹		-1.71	351	-2.35		-7.21	294	-2.36
1760	-378.1	-9.71	-2.28 ⁹		-1.54	355	-2.26		-6.74	297	-2.27
1600	-429.55	-11.98	-2.59 ³²		-1.70	359	-2.59		-7.30	300	-2.61
2000	-304	-6.99	-2.02 ³³		-1.34	356	-2.00		-6.02	297	-2.02

The experimental oxygen chemical potential and oxygen partial pressure are also reported. The computed values refer to the 1Cr+1Ov (M1) and 2Cr+2Ov (M2) models and we used the computed reaction enthalpy, $\Delta H = 327 \text{ kJ mol}^{-1}$ and 384 kJ mol^{-1} , respectively. In addition we report the ΔH values fitted to the experimental data, and the resulting maximum solubility (y_e) obtained with these values. The uncertainties in the measured solubilities are estimated at 7%⁴.

measured solubilities and that the perfect match could be obtained with the reaction enthalpy increased by only $\sim 21 \text{ kJ mol}^{-1}$. This is an excellent agreement, keeping in mind computational uncertainty of $\sim 50 \text{ kJ mol}^{-1}$ ²². On the other hand, in the case of 2Cr+2Ov model, the computed ΔH is by $\sim 90 \text{ kJ mol}^{-1}$ larger than the value that matches the maximum solubility data. The good description of the Cr solubility data with the 1Cr+1Ov model is yet another argument supporting the Cr^{2+} scenario found in our atomistic modeling studies and by the re-evaluation of the XANES data, pointing towards 1Cr+1Ov structural arrangements as a realistic case. In the next step, we will check how that structure matches the measured lattice parameters of Cr-doped UO_2 .

Lattice parameter of Cr-doped UO_2 . It is established experimentally that the UO_2 matrix doped with Cr undergoes contraction. The two available experimental studies of Leenaers et al.⁹ and Cardinaels et al.¹ show linear decrease of the lattice parameter with content of Cr, with the amount of incorporated chromium of up to $1000 \mu\text{g g}^{-1}$. The measured relative decrease of lattice parameter, reported in Table 5, varies by a factor of 2 between the two experimental studies, but in both cases is smaller than the one expected from consideration of sizes of the involved species⁹. In Table 5 we also report the simulated change in the lattice parameter obtained for all the considered structures (Fig. 2). Interestingly, the 1Cr+1Ov (a) and 2Cr+2Ov (a) structures result in very small shift and the result obtained for 1Cr+1Ov (a) structure matches the measured data. The other structures, including the 2Cr+1Ov configuration, result in significantly, at least order of magnitude larger change. We note however, that most of the configurations, except 2Cr+1Uv and 2Cr+2Ov (a) cases, predict decrease of the lattice parameter. The small, and well consistent with the measurements, lattice contraction with 1Cr+1Ov (a) structure is thus yet another argument that this is the correct Cr incorporation model.

Discussion

Using the accurate first principles method we performed intensive ab initio calculations of chromium-doped UO_2 matrix that represents an enhanced nuclear fuel case. In spite of trying to obtain the Cr^{3+} oxidation state, either by co-formation of U^{5+} or creation of oxygen vacancies, we always ended up with the Cr^{2+} state. The consideration of U^{4+} , Cr^{3+} , and Cr^{2+} cations sizes shows that Cr^{2+} has much similar size to U^{4+} and Cr^{3+} is much smaller, indicating plausibility of Cr^{2+} scenario. The goodness of such, nevertheless, rather-unexpected prediction has been further demonstrated by the re-evaluation of the measured XANES with the previously omitted reference for Cr^{2+} species. The calculations show that the most thermodynamically favorable structure is with an associated pair of Cr atom and oxygen vacancy. In such

Table 5 The computed and measured relative change of lattice parameter a ($\Delta a/a$) in Cr-doped UO_2 with Cr content of $1000 \mu\text{g g}^{-1}$.

Configuration	$\Delta a/a \cdot (\times 10^{-3})$
1Cr	-1.72
2Cr+1Ov	-1.41
1Cr + 1Ov (a)	-0.25
1Cr+1Ov (b)	-1.07
2Cr+2Ov (a)	+0.02
2Cr+2Ov (b)	-0.79
2Cr+1Uv (Uvac, Uvac)	+1.42
2Cr+1Uv (U, Uvac)	+0.71
Exp. ⁹	-0.12
Exp. ¹	-0.22

The bold face font indicates the result for thermodynamically favorable structure (see Table 3).

a configuration, Cr atom is shifted towards cations sublattice vacant site, which results in reduced, pseudo sixfold coordination, as opposite to the eightfold coordinated uranium site. The thermodynamic consideration of such a structure results in a good match to the measured maximum solubility of Cr in UO_2 and the small lattice contraction of Cr-doped UO_2 . This strongly indicates that we not only obtained a correct description of Cr oxidation state as “+2” valence state, but also good understanding of the structural incorporation of Cr into the UO_2 matrix. In these aspects the obtained results should be very helpful for correct interpretation of the measurements of Cr-doped UO_2 nuclear fuel. We hope that our studies will trigger supplementary investigations of not always intuitive redox solid state chemistry and structural/thermodynamic parameters of doped nuclear fuel matrices.

The reported results come from the synergy of atomistic modeling and data collected by different experimental techniques. A careful choice of the accurate computational method allowed for making an unexpected prediction regarding the oxidation state of Cr, which initiated the re-evaluation of the experimental data. This shows the need of atomistic modeling support for correct interpretation of the measurements and thus in-depth, correct understanding of challenging electronic systems such as, for instance, the doped UO_2 matrices.

Methods

Density functional theory (DFT) simulations. The DFT-based ab initio calculations were performed with the DFT-based plane-wave Quantum-ESPRESSO package³⁶. In DFT calculations, we specifically applied the gradient-corrected PBEsol exchange correlation functional³⁷ because it results in a good description of structures of f -element-bearing materials^{22,38,39} and a good prediction of their vibrational^{40,41} and thermodynamic parameters^{25,42}. We applied the scalar

relativistic ultrasoft pseudopotentials to mimic the presence of core electrons of the considered atoms⁴³. We note that in the case of uranium, the spin-orbit effects are of secondary importance and can be neglected^{22,44}. As a result of our previous extensive tests studies, we applied the plane-wave cut-off energy of 50 Ryd²². The computed $2 \times 2 \times 2$ supercell of UO_2 contained 96 atoms and the Brillouin zone was sampled with the $2 \times 2 \times 2$ Methfessel-Paxton k -points grid⁴⁵. The size of the computed system and the k -points sampling are similar to the simulation setup used in the previous studies^{6,46–48}. The lattice parameters and the atomic positions in all the computed structures were relaxed to the equilibrium positions, assuming constant pressure of $P = 0$ GPa with a tolerance of 0.1 GPa. The computed atomic structure is visualized in Fig. 1. It is of cubic fluorite-type with eightfold coordinated U atoms. As U and Cr atoms contain strongly correlated electrons, $5f$ and $3d$, respectively, we applied the DFT+ U method and derived the Hubbard U parameter from first principles using the linear response method⁴⁹. This method is known to give accurate values for $3d$ elements^{50,51} and has been extensively tested by us for f elements and subsequently applied to describe the electronic structure of uranium oxides, including UO_2 (e.g., refs. 15,22,38). Following the recent studies of Pegg et al.⁵², all the calculations were performed assuming anti-ferromagnetic transverse 1k spins arrangement in UO_2 . This resulted in a small distortion towards tetrahedral symmetry ($\sim 0.3\%$ of the lattice parameter value). Computation of the correct ground state of UO_2 is a challenge by itself and to assure the convergence to the correct ground state we applied the occupation matrix control technique⁵³. After the tests performed by Beridze and Kowalski²² for uranium-based compounds, we estimate the uncertainty of the so computed solid state reaction enthalpies at the level of ~ 50 kJ mol⁻¹.

Molecular dynamic simulations. In order to probe the possible structural arrangements of Cr atoms within the UO_2 matrix, focusing on the potential distortions of the computed atomic arrangements, we performed a set of test, qualitative level classical molecular dynamics simulations runs using GULP code⁵⁴. For such purpose we applied the simple Buckingham-type pair potentials of Lewis and Catlow⁵⁵ for the Cr^{2+} -O, U^{4+} -O and O-O interactions. We also performed simulations with the more accurate Embedded Atom Model (EAM) force fields developed specifically for UO_2 system by Cooper and Grimes⁵⁶. In the second case we adjusted the parameters of Cr^{2+} -O Buckingham-type pair potential to match the lattice parameters and the atomic arrangements of CrO solid, for the charge of Cr^{2+} of +1.1104 imposed by the charges of U (+2.2208) and O (-1.1104) in the EAM potential of Cooper and Grimes⁵⁶. We note that simple Buckingham-type potentials can not be expected to provide accurate (e.g., at the ab initio calculations level) structural parameters or energies and that mixing of the interaction potentials of different types is not always well grounded. However, we used the molecular dynamics simulations only to explore potential structural distortions of the computed structural arrangements of Cr in UO_2 and these simulations were not used to derive any numbers or structural/thermodynamic parameters discussed in the paper. The molecular dynamics NPT (constant pressure-temperature) runs were performed using standard approach (e.g., ref. 12). These were 20 ps long, with time step of 0.001 ps, and were performed at $T = 1000$ K and $P = 0$ GPa, both controlled by the thermostat.

Data availability

All the relevant data are available from the authors upon request.

Received: 13 November 2019; Accepted: 26 February 2020;

Published online: 23 March 2020

References

- Cardinaels, T. et al. Chromia doped uO_2 fuel: investigation of the lattice parameter. *J. Nucl. Mater.* **424**, 252–260 (2012).
- Arborelius, J. et al. Advanced doped uO_2 pellets in lwr applications. *J. Nucl. Sci. Technol.* **43**, 967–976 (2006).
- Peres, V. et al. High temperature chromium volatilization from cr_2o_3 powder and cr_2o_3 -doped uO_2 pellets in reducing atmospheres. *J. Nucl. Mater.* **423**, 93–101 (2012).
- Riglet-Martial, C. et al. Thermodynamics of chromium in uO_2 fuel: a solubility model. *J. Nucl. Mater.* **447**, 63–72 (2014).
- Yang, J. H. et al. Effect of step wise variation of oxygen potential during the isothermal sintering on the grain growth behavior in cr_2o_3 doped uO_2 pellets. *J. Nucl. Mater.* **429**, 25–33 (2012).
- Cooper, M., Stanek, C. R. & Andersson, D. The role of dopant charge state on defect chemistry and grain growth of doped uO_2 . *Acta Mater.* **150**, 403–413 (2018).
- Mieszczynski, C. et al. Microbeam x-ray absorption spectroscopy study of chromium in large-grain uranium dioxide fuel. *J. Phys. Condens. Matter* **26**, 355009 (2014).
- Lunk, H.-J. Discovery properties and applications of chromium and its compounds. *ChemTexts* **1**, 6 (2015).
- Leenaers, A., de Tollenaere, L., Delafoye, C. & den Bergh, S. V. On the solubility of chromium sesquioxide in uranium dioxide fuel. *J. Nucl. Mater.* **317**, 62–68 (2003).
- Jahn, S. & Kowalski, P. M. Theoretical approaches to structure and spectroscopy of earth materials. *Rev. Mineral. Geochem.* **78**, 691 (2014).
- Guo, Z., Ngayam-Happy, R., Krack, M. & Pautz, A. Atomic-scale effects of chromium-doping on defect behaviour in uranium dioxide fuel. *J. Nucl. Mater.* **488**, 160–172 (2017).
- Middleburgh, S. et al. Solution of trivalent cations into uranium dioxide. *J. Nucl. Mater.* **420**, 258–261 (2012).
- Kvashnina, K. O., Butorin, S. M., Martin, P. & Glatzel, P. Chemical state of complex uranium oxides. *Phys. Rev. Lett.* **111**, 253002 (2013).
- Sanyal, K., Khooha, A., Das, G., Tiwari, M. K. & Misra, N. L. Direct determination of oxidation states of uranium in mixed-valent uranium oxides using total reflection x-ray fluorescence x-ray absorption near-edge spectroscopy. *Anal. Chem.* **89**, 871–876 (2017).
- Kvashnina, K. O. et al. Trends in the valence band electronic structures of mixed uranium oxides. *Chem. Commun.* **54**, 9757–9760 (2018).
- Shoosmith, D., Sunder, S., Bailey, M. & Wallace, G. The corrosion of nuclear fuel (uO_2) in oxygenated solutions. *Corros. Sci.* **29**, 1115–1128 (1989).
- Ewing, R. C. Long-term storage of spent nuclear fuel. *Nat. Mater.* **14**, 252–257 (2015).
- Wang, J. & Gong, X.-Q. A dft+u study of v, cr and mn doped $\text{ceO}_2(111)$. *Appl. Surf. Sci.* **428**, 377–384 (2018).
- Mann, G. W., Lee, K., Cococcioni, M., Smit, B. & Neaton, J. B. First-principles hubbard u approach for small molecule binding in metal-organic frameworks. *J. Chem. Phys.* **144**, 174104 (2016).
- Wang, L., Maxisch, T. & Ceder, G. Oxidation energies of transition metal oxides within the GGA + U framework. *Phys. Rev. B* **73**, 195107 (2006).
- Wang, Y. et al. First-principles lattice dynamics, thermodynamics, and elasticity of cr_2o_3 . *Surf. Sci.* **606**, 1422–1425 (2012).
- Beridze, G. & Kowalski, P. M. Benchmarking the dft+u method for thermochemical calculations of uranium molecular compounds and solids. *J. Phys. Chem. A* **118**, 11797–11810 (2014).
- Vitova, T. et al. Dehydration of the uranyl peroxide studtite, $[\text{uO}_2(\eta^2-\text{o}_2)(\text{h}_2\text{o})_2] \cdot 2\text{h}_2\text{o}$, affords a drastic change in the electronic structure: a combined x-ray spectroscopic and theoretical analysis. *Inorg. Chem.* **57**, 1735–1743 (2018).
- Shannon, R. Revised effective ionic radii and systematic studies of interatomic distances in halides and chalcogenides. *Acta Cryst. Sec. A* **32**, 751–767 (1976).
- Kowalski, P. M. & Li, Y. Relationship between the thermodynamic excess properties of mixing and the elastic moduli in the monazite-type ceramics. *J. Eur. Ceram. Soc.* **36**, 2093–2096 (2016).
- Henderson, G. S., de Groot, F. M. F. & Moulton, B. J. A. In *Spectroscopic Methods in Mineralogy and Materials Sciences*, Vol. 78 (eds Henderson, G., Neuville, D. & Downs, R.) 75–138 (The Mineralogical Society of America, Virginia, 2015).
- Farges, F. Chromium speciation in oxide-type compounds: application to minerals, gems, aqueous solutions and silicate glasses. *Phys. Chem. Miner.* **36**, 463–481 (2009).
- Eeckhout, S. G., Bolfan-Casanova, N., McCammon, C., Klemme, S. & Amiguet, E. XANES study of the oxidation state of Cr in lower mantle phases: periclase and magnesium silicate perovskite. *Am. Mineral.* **92**, 966–972 (2007).
- Wilke, M., Farges, F., Petit, P.-E., Brown, G. & Martin, F. Oxidation state and coordination of Fe in minerals: an Fe K-XANES spectroscopic study. *Am. Mineral.* **86**, 714–730 (2001).
- Tocino, F., Szenknect, S., Mesbah, A., Clavier, N. & Dacheux, N. Dissolution of uranium mixed oxides: the role of oxygen vacancies vs the redox reactions. *Prog. Nucl. Energy* **72**, 101–106 (2014).
- Inoue, A. & Tsujino, T. Dissolution rates of uranium oxide ($\text{u}_3\text{o}_8\text{u}_3\text{o}_9$) powders in nitric acid. *Ind. Eng. Chem. Process Des. Dev.* **23**, 122–125 (1984).
- Bourgeois, L., Dehaut, P., Lemaignan, C. & Hammou, A. Factors governing microstructure development of $\text{cr}_2\text{o}_3\text{cr}_2\text{o}_3$ -doped uO_2 during sintering. *J. Nucl. Mater.* **297**, 313–326 (2001).
- Kleykamp, H. Phase equilibria in the uO_2 -austenitic steel system up to 3000 °C. *J. Nucl. Mater.* **247**, 103–107 (1997).
- Chase, J. M. W. *NIST-JANAF Thermochemical Tables, 4th edn.*, Vol. 9 (American Institute of Physics, 1998).
- Toker, N. Y., Darken, L. S. & Muan, A. Equilibrium phase relations and thermodynamics of the Cr-O system in the temperature range of 1500 °C to 1825 °C. *Metall. Trans. B* **22**, 225–232 (1991).
- Giannozzi, P. et al. Quantum espresso: a modular and open-source software project for quantum simulations of materials. *J. Phys.: Condens. Matter* **21**, 395502–395520 (2009).
- Perdew, J. P. et al. Restoring the density-gradient expansion for exchange in solids and surfaces. *Phys. Rev. Lett.* **100**, 136406 (2008).
- Blanca-Romero, A., Kowalski, P. M., Beridze, G., Schlenz, H. & Bosbach, D. Performance of dft plus u method for prediction of structural and

- thermodynamic parameters of monazite-type ceramics. *J. Comput. Chem.* **35**, 1339–1346 (2014).
39. Beridze, G., Birnie, A., Koniski, S., Ji, Y. & Kowalski, P. M. Dft+u as a reliable method for efficient ab initio calculations of nuclear materials. *Prog. Nucl. Energy* **92**, 142–146 (2016).
 40. Kowalski, P. M., Beridze, G., Vinograd, V. L. & Bosbach, D. Heat capacities of lanthanide and actinide monazite-type ceramics. *J. Nucl. Mater.* **464**, 147–154 (2015).
 41. Ji, Y., Beridze, G., Bosbach, D. & Kowalski, P. M. Heat capacities of xenotime-type ceramics: an accurate ab initio prediction. *J. Nucl. Mater.* **494**, 172–181 (2017).
 42. Li, Y., Kowalski, P. M., Blanca-Romero, A., Vinograd, V. & Bosbach, D. Ab initio calculation of excess properties of solid solutions. *J. Solid State Chem.* **220**, 137–141 (2014).
 43. Vanderbilt, D. Soft self-consistent pseudopotentials in a generalized eigenvalue formalism. *Phys. Rev. B* **41**, 7892 (1990).
 44. Shamov, G. A., Schreckenbach, G. & Vo, T. N. A comparative relativistic dft and ab initio study on the structure and thermodynamics of the oxofluorides of uranium (iv), (v) and (vi). *Chem. Eur. J.* **13**, 4932–4947 (2007).
 45. Methfessel, M. & Paxton, A. T. High-precision sampling for brillouin-zone integration in metals. *Phys. Rev. B* **40**, 3616 (1989).
 46. Crocombette, J.-P. Influence of charge states on energies of point defects and clusters in uranium dioxide. *Phys. Rev. B* **85**, 144101 (2012).
 47. Crocombette, J.-P. First-principles study with charge effects of the incorporation of iodine in uo₂. *J. Nucl. Mater.* **429**, 70–77 (2012).
 48. Yang, J. H. et al. Effect of step wise variation of oxygen potential during the isothermal sintering on the grain growth behavior in cr₂o₃ doped uo₂ pellets. *J. Nucl. Mater.* **429**, 25–33 (2012).
 49. Cococcioni, M. & de Gironcoli, S. Linear response approach to the calculation of the effective interaction parameters in the LDA . U method. *Phys. Rev. B* **71**, 035105 (2005).
 50. Şaşıoğlu, E., Friedrich, C. & Blügel, S. Effective coulomb interaction in transition metals from constrained random-phase approximation. *Phys. Rev. B* **83**, 121101 (2011).
 51. Nakamura, K., Arita, R., Yoshimoto, Y. & Tsuneyuki, S. First-principles calculation of effective onsite coulomb interactions of 3d transition metals: constrained local density functional approach with maximally localized wannier functions. *Phys. Rev. B* **74**, 235113 (2006).
 52. Pegg, J. T. et al. Magnetic structure of uo₂ and npo₂ by first-principle methods. *Phys. Chem. Chem. Phys.* **21**, 760–771 (2019).
 53. Dorado, B., Amadon, B., Freyss, M. & Bertolus, M. DFT + U calculations of the ground state and metastable states of uranium dioxide. *Phys. Rev. B* **79**, 235125 (2009).
 54. Gale, J. D. Gulp: a computer program for the symmetry-adapted simulation of solids. *J. Chem. Soc., Faraday Trans.* **93**, 629–637 (1997).
 55. Lewis, G. V. & Catlow, C. R. A. Potential models for ionic oxides. *J. Phys. C: Solid State Phys.* **18**, 1149–1161 (1985).
 56. Cooper, M. W. D., Rushton, M. J. D. & Grimes, R. W. A many-body potential approach to modelling the thermomechanical properties of actinide oxides. *J. Phys.: Condens. Matter* **26**, 105401 (2014).

Acknowledgements

M.S. thanks CSC-China Scholarship Council for funding her Ph.D studies at Forschungszentrum Jülich in Germany. J.S. thanks DAAD-German Academic Exchange Service for funding his research stay at Forschungszentrum Jülich in Germany. We thank Victor Vinograd for comments on thermodynamic modeling used in this paper. Funded by the Excellence Initiative of the German federal and state governments and the Jülich Aachen Research Alliance-High-Performance Computing. We thank the JARA-HPC awarding body for time on the RWTH and Forschungszentrum Jülich computing resources awarded through JARA-HPC Partition.

Author contributions

The ab initio calculations and analysis of the results were performed by M.S., P.M.K., and J.S. The re-evaluation of the XANES data, including fitting procedure and the analysis, was performed by M.S. and J.S. P.M.K. performed the thermodynamic modeling and led the project. All parties participated in writing the manuscript.

Competing interests

The authors declare no competing interests.

Additional information

Supplementary information is available for this paper at <https://doi.org/10.1038/s43246-020-0014-5>.

Correspondence and requests for materials should be addressed to P.M.K.

Reprints and permission information is available at <http://www.nature.com/reprints>

Publisher's note Springer Nature remains neutral with regard to jurisdictional claims in published maps and institutional affiliations.



Open Access This article is licensed under a Creative Commons Attribution 4.0 International License, which permits use, sharing, adaptation, distribution and reproduction in any medium or format, as long as you give appropriate credit to the original author(s) and the source, provide a link to the Creative Commons license, and indicate if changes were made. The images or other third party material in this article are included in the article's Creative Commons license, unless indicated otherwise in a credit line to the material. If material is not included in the article's Creative Commons license and your intended use is not permitted by statutory regulation or exceeds the permitted use, you will need to obtain permission directly from the copyright holder. To view a copy of this license, visit <http://creativecommons.org/licenses/by/4.0/>.

© The Author(s) 2020